

Paper:

Measurement of Three-Dimensional Environment with a Fish-Eye Camera Based on Structure from Motion - Error Analysis

Kenji Terabayashi^{*,**}, Hisanori Mitsumoto^{***}, Toru Morita^{*}, Yohei Aragaki^{****}, Noriko Shimomura^{****}, and Kazunori Umeda^{*,**}

^{*}Dept. of Precision Mechanics, Faculty of Science and Engineering, Chuo University
1-13-27 Kasuga, Bunkyo-ku, Tokyo 112-8551, Japan
E-mail: terabayashi@mech.chuo-u.ac.jp

^{**}CREST Program, Japan Science and Technology Agency (JST)

^{***}Toyota Motor Corporation

375-1 Imazato, Susono, Shizuoka 410-1104, Japan

^{****}Nissan Motor Co.,Ltd.

1-1 Morinosatoayama, Atsugi-shi Kanagawa 243-0123, Japan

[Received June 2, 2009; accepted September 30, 2009]

This paper proposes a method for measuring 3-dimensional (3D) environment and estimating camera movement with two fish-eye images. This method deals with large distortion of images from a fish-eye camera to calibrate internal and external camera parameters precisely by simultaneous estimation. In this paper, we analyze 3D measurement accuracy based on a theoretical model and evaluate it in practical analysis in experimental and real environments. These analyses show that the theoretical measurement error model works over a wide range of fish-eye views.

Keywords: fish-eye, structure from motion, three dimensional measurement, error analysis

1. Introduction

To get images of wide field of view, there are several types of cameras - omnidirectional [1, 2], spherical [3], and fish-eye [4, 5] - capture the wide-field images used in robot and car-driver support applications. The fish-eye camera is most appropriate in driving support system for the following reasons. The first one is the installed position of cameras. Both omnidirectional and spherical cameras restrict the position to special locations such as on the top of a car. The second one is the directivity of captured image resolution. The fish-eye camera on the front of a vehicle has the same view as the driver [6].

In related work, Shigang and Shimomura [4] developed a system for lane marking detection with side fish-eye camera, although this was restricted to 2-dimensional line on the ground. The fish-eye stereo camera system proposed by Gehrig et al [5] and Nishimoto et al [7] measures a 3-dimensional (3D) environment but is too costly for vehicle installation. Xiaoming et al [8] proposed spherical

panorama generation with two fish-eye images for immersive display in virtual reality, but measurement accuracy was not considered.

We propose 3D measurement with two images captured by a single fish-eye camera by estimating camera movement, and analyze accuracy based on a theoretical model. We deal with large distortion of fish-eye image by calibrating internal and external camera parameters precisely and simultaneously.

This paper is organized as follows: Section 2 introduces a fish-eye camera projection model. Section 3 outlines our proposal. Section 4 details our algorithm to measure 3D environment by estimating camera movement. Section 5 discusses measurement accuracy theoretically and experimentally in Sections 6 and 7. Section 8 summarizes conclusions.

2. Fish-Eye Camera Model

Fish-eye lens projection changes with the objective of use. Typical projection models are the following four:

(i). Equidistance projection:

$$r_f = \delta \theta \quad \dots \dots \dots (1)$$

(ii). Orthogonal projection:

$$r_f = \delta \sin \theta \quad \dots \dots \dots (2)$$

(iii). Stereographic projection:

$$r_f = 2\delta \tan(\theta/2) \quad \dots \dots \dots (3)$$

(iv). Equisolid angle projection:

$$r_f = 2\delta \sin(\theta/2) \quad \dots \dots \dots (4)$$

r_f is the distance from the projection point to the lens axis and θ is the angle formed by the projection line and the lens axis. Parameter δ is the following ratio of focal length f [mm] and pixel size w [mm]:

$$\delta = f/w. \quad \dots \quad (5)$$

However, general-purpose fish-eye lens projection cannot be represented by the above projection models because of the influence of in-process noise, etc. In this study, we define the fish-eye camera model as the following 5th polynomial:

$$r_f = k_1\theta + k_3\theta^3 + k_5\theta^5. \quad \dots \quad (6)$$

$k_a(a = 1, 3, 5)$ is an internal camera parameter. In consideration of the gap between the optical axis and the center of a CCD element, the internal parameters are defined as follows:

$$\mathbf{I} = [k_1 \ k_3 \ k_5 \ c_u \ c_v]^T. \quad \dots \quad (7)$$

(c_u, c_v) is the relative position of optical axis. These parameters are estimated precisely as described in previous work [9].

3. Overview

Modeling a 3D environment using a fish-eye camera and estimating camera movement involve the following 6 steps, as shown in **Fig. 1**:

- (i). Two images are captured by the fish-eye camera at different observation points during camera movement.
- (ii). Corresponding feature points are searched for and extracted from the images.
- (iii). Camera movement is estimated using information of corresponding feature points.
- (iv). 3D positions of feature points are calculated using estimated camera movement based on the principle of triangular surveying.
- (v). Camera movement precision is improved using bundle adjustment [10].
- (vi). 3D positions of feature points are recalculated using optimized camera movement generating a 3D environment model with color information.

4. 3D Measurement

4.1. Search for Corresponding Points

Corresponding points are searched for in images in the fish-eye image sequence. Feature points - a corner and an edge point for example - are extracted from the first image and tracked along the sequence. We use Lucas Kanade (LK) tracker algorithm with pyramid representation [11]

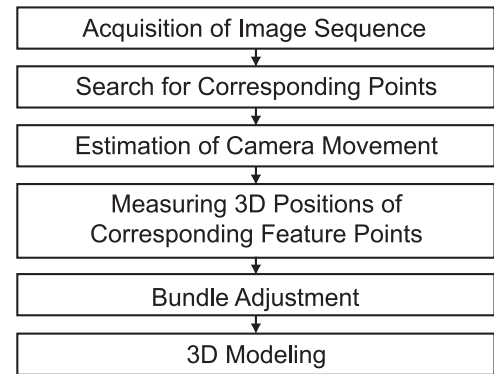


Fig. 1. Outline of 3D measurement.

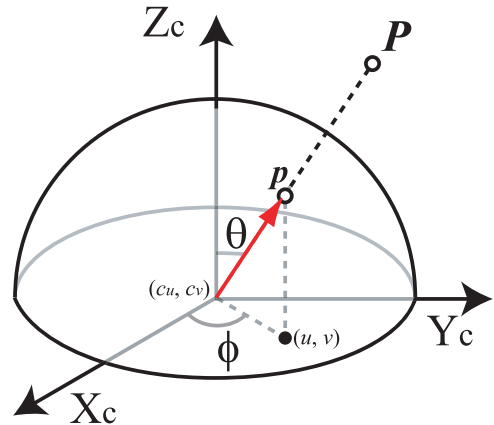


Fig. 2. Sphere model and ray vector definition.

indoors because it is easier to calculate congruent points than outdoors. We use the Scale-Invariant Feature Transform (SIFT) [12] algorithm outdoors despite the high calculation cost because it calculates corresponding points more precisely than the LK-tracker.

4.2. Ray Vector Calculation

As shown in **Fig. 2**, we define an unit vector as a ray vector whose direction is from the lens center of the camera toward an object point in 3D space. The ray vector of fish-eye camera is given as follows:

$$\mathbf{p} = [\sin \theta \cos \phi \quad \sin \theta \sin \phi \quad \cos \theta]^T. \quad \dots \quad (8)$$

θ is the zenith angle and ϕ is the azimuthal angle, as shown in **Fig. 2**. These angles are calculated from image coordinates $[u, v]^T$ of the feature point as follows:

$$k_1\theta + k_3\theta^3 + k_5\theta^5 - \sqrt{(u - c_u)^2 + (v - c_v)^2} = 0 \quad (9)$$

$$\phi = \tan^{-1} \left(\frac{v - c_v}{u - c_u} \right). \quad \dots \quad (10)$$

The zenith angle may have more than one solution but the solution must have the consistency of angular constraint within a range from 0 to $\pi/2$ rad. This angle is calculated using the Van Wijngaarden-Dakker-Brent method [13].

4.3. Essential Matrix Calculation

Essential matrix \mathbf{E} is calculated using ray vectors $\mathbf{p}_i = [x_i, y_i, z_i]^T$ and $\mathbf{p}'_i = [x'_i, y'_i, z'_i]^T$, which are those of the corresponding points in the two images [14]. This matrix has information on the camera motion direction and rotation, so camera movement is calculated by matrix \mathbf{E} . The relationship between essential matrix \mathbf{E} and ray vector \mathbf{p} is given as follows:

$$\mathbf{p}_i'^T \mathbf{E} \mathbf{p}_i = 0. \quad \dots \quad (11)$$

Eq. (11) is transformed as follows:

$$\mathbf{u}_i^T \mathbf{e} = 0 \quad \dots \quad (12)$$

where

$$\mathbf{u}_i = [x_i x'_i, y_i x'_i, z_i x'_i, x_i y'_i, y_i y'_i, z_i y'_i, x_i z'_i, y_i z'_i, z_i z'_i]^T, \\ \mathbf{e} = [e_{11}, e_{12}, e_{13}, e_{21}, e_{22}, e_{23}, e_{31}, e_{32}, e_{33}]^T.$$

Parameter e_{ij} is the row i and column j element of matrix \mathbf{E} . The matrix has 9 elements and the matrix scale is arbitrary, so essential matrix \mathbf{E} is obtained by solving simultaneous equations for at least 8 pairs of corresponding ray vectors.

4.4. Outlier Removal

Data on corresponding points tracked between two images may include points of mis-tracking adversely affect results for essential matrix \mathbf{E} and camera movement estimation. We use the random sample consensus (RANSAC) [15] to remove these points as outliers as follows:

- (i). Eight feature points are randomly chosen and.
- (ii). essential matrix \mathbf{E} is calculated as described above.
- (iii). Using ray vectors $\mathbf{p}_i, \mathbf{p}'_i$ in two images, the number k of feature points satisfying Eq. (13) is counted:

$$|\mathbf{p}_i'^T \mathbf{E}_{rand} \mathbf{p}_i| < q \quad \dots \quad (13)$$

q is a threshold.

- (iv). Steps (i)-(iii) are repeated 20 times.
- (v). For the maximum number of k , feature points not satisfying Eq. (13) are removed as outliers.

Essential matrix \mathbf{E} is calculated using remaining feature points.

4.5. Camera Motion Estimation

Camera movement is estimated from essential matrix \mathbf{E} using the relationship between essential matrix \mathbf{E} and translation vector $\mathbf{t} = [t_x, t_y, t_z]^T$ given by:

$$\mathbf{E}^T \mathbf{t} = 0. \quad \dots \quad (14)$$

Vector $\bar{\mathbf{t}}$, which is the unit vector of \mathbf{t} calculated above, is the eigenvector to the minimum eigenvalue of matrix

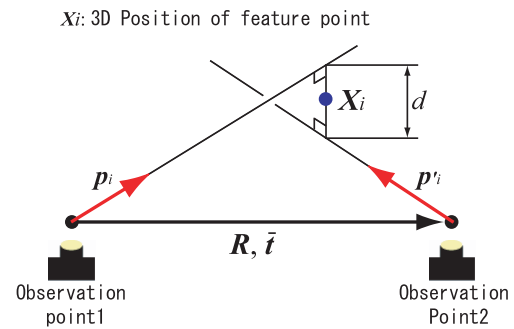


Fig. 3. Measurement of 3D position.

$\mathbf{E}\mathbf{E}^T$. For camera rotation, the relationship between essential matrix \mathbf{E} and rotation matrix \mathbf{R} is as follows:

$$\bar{\mathbf{E}} = [\bar{\mathbf{t}}]_{\times} \mathbf{R} \quad \dots \quad (15)$$

$$[\bar{\mathbf{t}}]_{\times} = \begin{bmatrix} 0 & -t_z & t_y \\ t_z & 0 & -t_x \\ -t_y & t_x & 0 \end{bmatrix} \quad \dots \quad (16)$$

For Eq. (15), matrix \mathbf{R} is the solution minimizing

$$c_1 = \|\bar{\mathbf{E}} - [\bar{\mathbf{t}}]_{\times} \mathbf{R}\|^2. \quad \dots \quad (17)$$

Symbol $\|\cdot\|$ is the Frobenius norm, and Eq. (17) is solved using a quaternion.

4.6. 3D Measurement

3D positioning of object points $\mathbf{X}_i = [X_i, Y_i, Z_i]^T$ projected as feature points in the image are calculated using translation vector $\bar{\mathbf{t}}$ and rotation matrix \mathbf{R} . 3D positioning of an object point is the intersection of the two ray vectors in two images, but noise may prevent this intersection, so 3D coordinate \mathbf{X}_i is defined as the point at which the sum of squares of the Euclidian distance from point \mathbf{X}_i to the two lines is minimized (Fig. 3). 3D positioning of feature points are calculated as follows:

$$\mathbf{X}_i = \mathbf{B}^{-1} \mathbf{b} \quad \dots \quad (18)$$

$$\mathbf{B} = 2\mathbf{I} - \frac{\mathbf{p}_i \mathbf{p}_i^T}{\mathbf{p}_i^T \mathbf{p}_i} - \frac{\mathbf{R} \mathbf{p}'_i \mathbf{p}'_i{}^T \mathbf{R}^T}{\mathbf{p}'_i{}^T \mathbf{p}'_i} \quad \dots \quad (19)$$

$$\mathbf{b} = \left(\mathbf{I} - \frac{\mathbf{R} \mathbf{p}'_i \mathbf{p}'_i{}^T \mathbf{R}^T}{\mathbf{p}'_i{}^T \mathbf{p}'_i} \right) \bar{\mathbf{t}}. \quad \dots \quad (20)$$

4.7. Inaccurate-Point Removal

Measurement accuracy become worse as object points approach the baseline direction or go far from the camera. Points with different accuracy are included in measurement data, so to restrict use to high-accuracy data alone, the measurement accuracy evaluation function is defined as follows [2]:

$$\mathbf{g} = \left| \frac{\partial \mathbf{X}_i}{\partial u_i} \right| + \left| \frac{\partial \mathbf{X}_i}{\partial v_i} \right| + \left| \frac{\partial \mathbf{X}_i}{\partial u'_i} \right| + \left| \frac{\partial \mathbf{X}_i}{\partial v'_i} \right|. \quad \dots \quad (21)$$

Vector \mathbf{g} is the sum of the absolute value that derives the partial differential of measurement result \mathbf{X}_i by image coordinates of two feature points $[u_i, v_i]^T, [u'_i, v'_i]^T$. Any point

at which vector \mathbf{g} does not satisfy Eq. (22) is removed because its measurement accuracy is low:

$$\|\mathbf{g}\| < h \quad \dots \quad (22)$$

where h is a threshold.

4.8. Bundle Adjustment

The above camera movement and 3D measurement data may not always yield good results because of image error. So we use bundle adjustment [10] to simultaneously optimize camera motion and measured 3D points by solving a nonlinear least squares problem using the estimated as initial values. This optimization is to minimize the sum of feature reprojection error, which is the difference between the original feature point coordinate in captured images and the coordinate with which 3D measurement data is projected to the image plane.

The image coordinates of reprojected feature points at two observation positions are calculated as follows:

$$\mathbf{u}_{b1} = \begin{bmatrix} u_{b1} \\ v_{b1} \end{bmatrix} = \frac{k_1\theta + k_3\theta^3 + k_5\theta^5}{\sqrt{X_i^2 + Y_i^2}} \begin{bmatrix} X_i \\ Y_i \end{bmatrix} \quad (23)$$

$$\mathbf{u}_{b2} = \begin{bmatrix} u_{b2} \\ v_{b2} \end{bmatrix} = \frac{k_1\theta' + k_3\theta'^3 + k_5\theta'^5}{\sqrt{X_i'^2 + Y_i'^2}} \begin{bmatrix} X_i' \\ Y_i' \end{bmatrix} \quad (24)$$

where

$$\theta = \tan^{-1} \left(\frac{\sqrt{X_i^2 + Y_i^2}}{Z_i} \right) \quad \dots \quad (25)$$

$$\theta' = \tan^{-1} \left(\frac{\sqrt{X_i'^2 + Y_i'^2}}{Z_i'} \right) \quad \dots \quad (26)$$

Coordinates $\mathbf{u}_{b1}, \mathbf{u}_{b2}$ are reprojected points in two images. Parameters $\mathbf{X}_i = [X_i, Y_i, Z_i]^T$ and $\mathbf{X}_i' = [X_i', Y_i', Z_i']^T$ are 3D coordinates of the feature point at each observation location. Parameter \mathbf{X}_i' is the coordinate for which coordinate conversion of parameter \mathbf{X}_i is done using translation vector \mathbf{t} and rotation matrix \mathbf{R} . We define the sum of feature reprojection errors as:

$$c_2 = \sum_{i=1}^n \sum_{j=1}^2 (\mathbf{u}_j - \mathbf{u}_{bj})^2 \quad \dots \quad (27)$$

c_2 is the sum of reprojection errors, \mathbf{u}_1 and \mathbf{u}_2 are original feature points coordinates in two images, and n is the sum of reprojected feature points. To minimize c_2 , we use the Levenberg Marquardt method [13]. In optimization using all feature points, calculation cost becomes expensive, so we use the RANSAC [15] as follows:

- (i). Several feature points - at least 6 - are randomly chosen.
- (ii). Using these feature points, camera movement is optimized and estimated.

- (iii). Using optimized camera movement, 3D locations are calculated for all feature points.
- (iv). Using 3D location data and optimized camera movement, feature reprojection errors c_2 is evaluated.
- (v). Step (i)-(iv) are repeated 20 times.
- (vi). The case in which c_2 is minimum is chosen and camera movement estimated at this time is determined as optimum.
- (vii). Using optimum camera movement, 3D locations are calculated for all feature points.

4.9. Texture Mapping

Generating a 3D model from 3D measurement data involves modeling using the Delaunay triangulation method to generate triangular meshes for obtained 3D measurement data. A texture image is pasted on each surface of the generated triangular mesh to construct a 3D model with color information.

5. Disturbance Model

To discuss accuracy of 3D measure with two fish-eye images, as shown in Fig. 4, we consider a case in which the camera moves in the direction of the optical axis.

Assuming that the distance d from the camera to a measuring point is sufficiently greater than the base length b_c , we develop the following based on geometric relationship:

$$d = \frac{b_c \sin \theta}{\Delta \theta} \quad \dots \quad (28)$$

where θ is the angle made by the projection line and the lens axis and $\Delta \theta$ is the difference of θ between observation points. If a propagation rule of error is applied to Eq. (28), uncertainty σ_d of the measurement distance is given as follows:

$$\sigma_d = \frac{d^2}{b_c \sin \theta} \sigma_{\Delta \theta} \quad \dots \quad (29)$$

$\sigma_{\Delta \theta}$ is $\Delta \theta$ uncertainty. We consider $\sigma_{\Delta \theta}$ as a constant, because d is sufficiently larger than b_c . From Eq. (29), the uncertainty of distance d is proportional to the square of d , and inversely proportional to $\sin \theta$.

6. Experimental Environment Error Analysis

Measurement errors are analyzed in two experiments based on the above disturbance model. The first experiment treats the central fish-eye image and the second focuses on the super-wide image angle area. These experiments are conducted in an experimental environment in which measurement points are easily controlled.

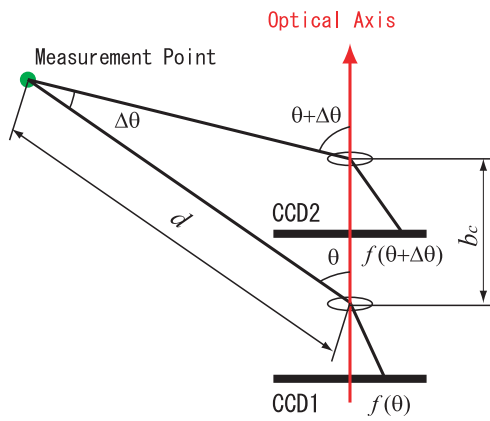


Fig. 4. Geometrical relationship between a measurement point and fish-eye camera moving toward optical axis.

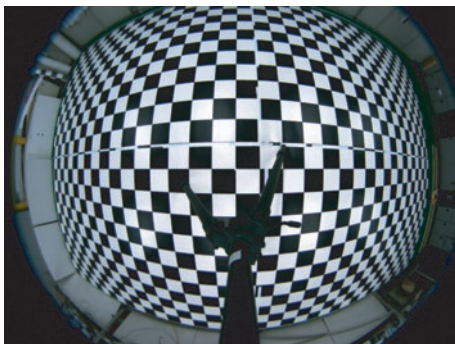


Fig. 5. Checkerboard sheet used for error analysis.

6.1. Error Analysis in Central Fish-Eye Images

It is verified whether our proposed method follows the above disturbance model of Eq. (29) for central area of fish-eye images. This experiment evaluates the disturbance model at distance d with θ fixed with θ_d based on d . When evaluating the model at θ , d is fixed with d_θ based on θ . These evaluations change the disturbance model of Eq. (29) to Eq. (30) at distance d , and to Eq. (31) at θ :

$$\sigma_d \sin \theta_d = \frac{d^2}{b_c} \sigma_{\Delta\theta} \quad \dots \dots \dots (30)$$

$$\frac{\sigma_d}{d_\theta^2} = \frac{1}{b_c \sin \theta} \sigma_{\Delta\theta} \quad \dots \dots \dots (31)$$

By verifying the disturbance model of Eqs. (30) and (31), we determine whether the proposed method follows the model of Eq. (29).

The 3D location of grid points on the checkerboard sheet shown in Fig. 5 are measured as targets. The size of the sheet is 3656 × 5292 mm. The CCD camera used is Dragonfly2 (Point-Grey-Research), and the fish-eye lens is TV1634M (SPACE). The internal camera parameter is set to a value estimated experimentally ($k_1 = 365.85$, $k_3 = -13.68$, $k_5 = -0.85$, $c_u = 10.14$, $c_v = 17.10$). The image size is 1024 × 768 pixels. The camera was set to make the optical axis perpendicular to the checkerboard sheet, and the camera and the sheet were placed 1000 mm apart. The base length of camera movement was 40 mm long.

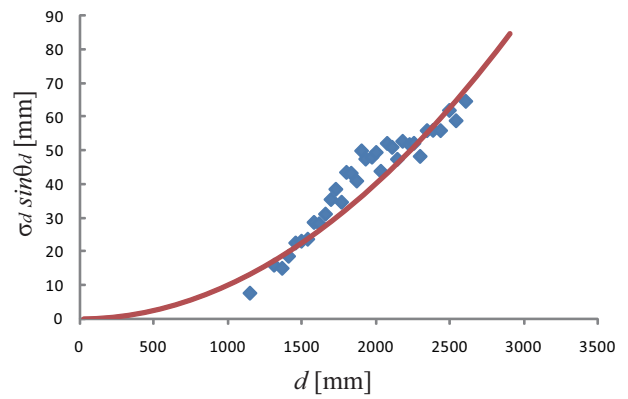


Fig. 6. Error analysis about d .

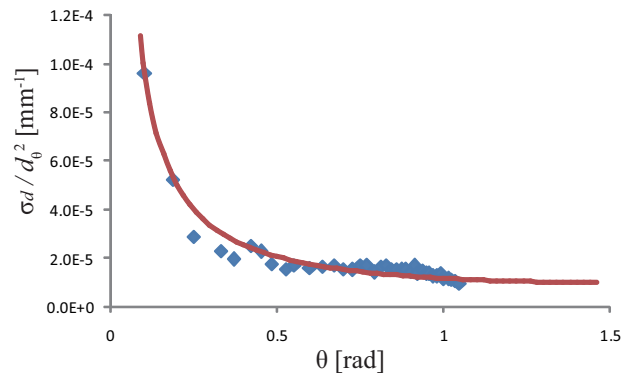


Fig. 7. Error analysis about θ .

3D measurement errors were analyzed by comparing the measured 3D position and ground truth. The origin of world coordinates was the camera lens center before movement. The 3D location of the feature point measured using our proposal has uncertainty of scale, so scale was specified using the ratio between designed and estimated camera movement parameters.

Error analysis results at d and θ are shown in Figs. 6 and 7. In these figures, the solid line shows the disturbance model and each point indicates measured error deviation calculated using nearest 15 data.

In Fig. 6, measurement error deviation tends to be proportional to the square of distance d , consistent with the disturbance model of Eq. (30). Since each measured error deviation in Fig. 7 was inversely proportional to $\sin \theta$, the result followed the disturbance model of Eq. (31). So the disturbance model of Eq. (29) is appropriate for for 3D measurement error of our proposal using two images captured by a fish-eye camera within “ $d = 1000 - 2800$ mm” and “ $\theta = 0.2 - 1.2$ rad.”

6.2. Error Analysis in Super-Wide Fish-Eye Image Angle

In the previous experiment, it was not clear whether the disturbance model of Eq. (29) was valid in a super-wide angle ($\theta > 1.4$ rad), so we conducted an error analysis experiment for this area.

In our experimental environment, measurement data for a wide angle area may not always be obtained from

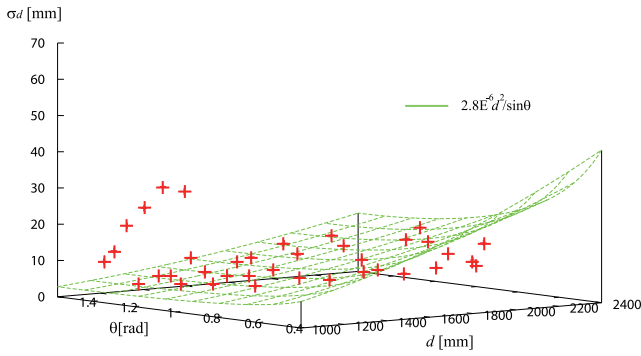


Fig. 8. Error analysis comparing theoretical disturbance model and measured error at $\theta - d$ space.

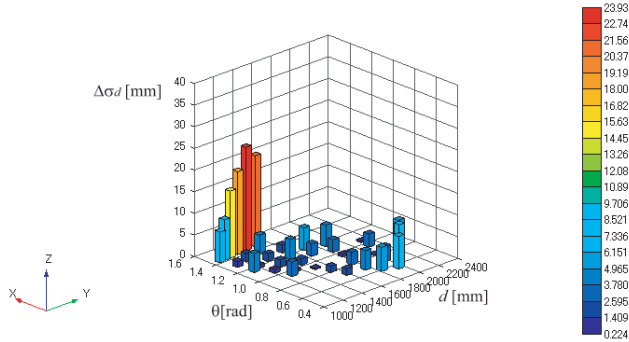


Fig. 9. Absolute difference in measured data σ_d and disturbance model.

one measurement. To obtain sufficient points to calculate measurement error deviation, 3D measurement was done at 8 observation points. Since dense measurement data can be acquired from multiple experiments, the disturbance model of Eq. (29) can be analyzed from the aspect of σ_d , d , and θ simultaneously.

The deviation of measurement error σ_d was calculated using data from 8 experiments, plotted in **Fig. 8** with the curve surface of the disturbance model of Eq. (29). Deviation σ_d was calculated using nearest 16 measurement data. **Fig. 8** shows that error deviation σ_d is proportional to the square to distance d and inversely proportional to $\sin \theta$ over a wide range of measurement, excluding super-wide angle area ($\theta > 1.4$ rad).

To verify the disturbance model easily, absolute difference $\Delta\sigma_d$ between the disturbance model and measured error deviation is shown in **Fig. 9**. This figure shows that the difference $\Delta\sigma_d$ is large in the super-wide angle.

Based on **Figs. 8** and **9**, the disturbance model of Eq. (29) is not appropriate for our proposal in super-wide angle ($\theta > 1.4$ rad) but appropriate in other areas for 2 reasons:

- (i). The disturbance model of Eq. (29) does not treat fish-eye lens distortion obviously, and
- (ii). the large distortion seen in super-wide angle ($\theta > 1.4$ rad) enlarges measurement error due to the low-resolution image.

These points indicate the importance of introducing fish-



Fig. 10. Input image captured in stair environment.

eye distortion models into new measurement error model as a future work.

Modifying fish-eye lens projection described in Section 2 is another way to improve the fitness of the error model. Kannala and Brandt [16] reported the importance of the tangential factor in the projection model of a fish-eye camera, so our projection model of Eq. (6) may require both radial and some tangential factors.

7. Actual Environment Error Analysis

We verified the disturbance model of Eq. (29) in actual environments in contrast to experimental environments in the previous section.

7.1. Experimental Setup

The experimental setup is the same as in Section 6. The fish-eye camera moved in the direction of the optical axis with base length $b_c = 100$ mm. Two fish-eye images were captured before and after camera movement as shown in **Fig. 10**, where stair environment was measured to verify the disturbance model in an actual environment. This is because this environment makes it easier to determine the 3D structure as ground truth than the general-purpose environment.

7.2. Experimental Results

Figure 11 shows the 3D model obtained from the two images. The appropriateness of the 3D model of the stair environment is confirmed in **Figs. 11 (a)** and **(b)**.

In this measurement result, measured stairs data was used to verify the disturbance model due to 2 reasons:

- (i). It was easy to calculate measurement error at each measured points because of the distance between these points and the plane along with stairs, and
- (ii). dense measured data could be obtained for calculating measured error deviation.

Figure 12 shows error analysis with the disturbance model and measured error deviation using stair data. The measured error deviation was calculated using close data

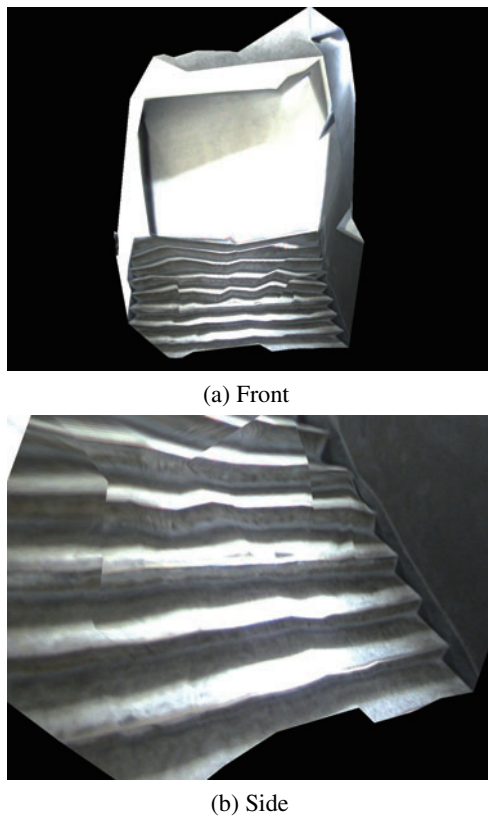


Fig. 11. 3D measurement result with texture.

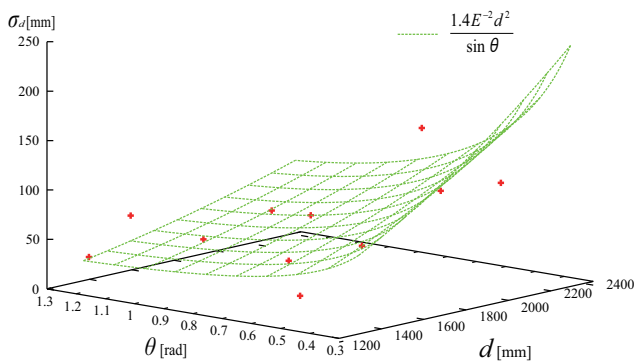


Fig. 12. Error analysis in an actual environment comparing theoretical disturbance model and measured error at $\theta - d$ space.

errors. This figure is sparser than the result for error analysis in an experimental environment, as shown in Fig. 8, due to the small number of measured points in the actual environment. This error analysis was done in the range of “ $d = 1200 - 2400$ mm” and “ $\theta = 0.3 - 1.3$ rad.” There is no data in a super-wide angle of fish-eye images ($\theta > 1.4$ rad).

To verify the disturbance model easily, the absolute difference $\Delta\sigma_d$ between the disturbance model and measured error deviation is shown in Fig. 13. This figure shows the variation of $\Delta\sigma_d$ is sufficiently small because the ratio to distance d is less than 5%.

The disturbance model of Eq. (29) was verified by this error analysis in an actual environment, consistent with previous experimental results.

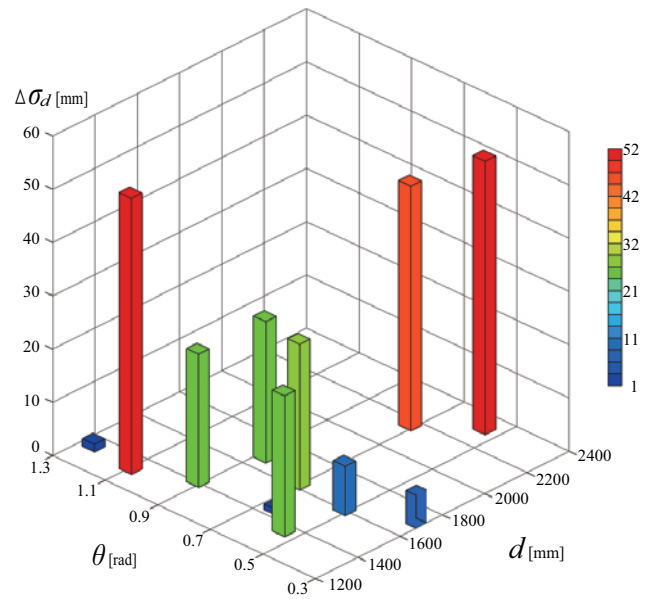


Fig. 13. Absolute difference in each data σ_d and disturbance model in an actual environment.

8. Conclusions

We have proposed measuring 3D environments using a single fish-eye camera. Measurement errors were analyzed theoretically and experimentally. A disturbance model developed theoretically for a camera moving in the direction of the optical axis was found to be verified in experimental and actual environments. Results showed that our method follows the disturbance model we developed in a wide range of fish-eye views except in a the super-wide angle.

Projected work includes expanding error analysis to structure from motion using multiple fish-eye images.

References:

- [1] R. Bunschoten and B. Krose, “Robust scene reconstruction from an omnidirectional vision system,” *IEEE Trans. on Robotics and Automation*, 19, pp. 351-357, 2003.
- [2] R. Kawanishi, A. Yamashita, and T. Kaneko, “Construction of 3D Environment Model from an Omni-Directional Image Sequence,” *Proc. 3rd Asia Int. Symposium on Mechatronics (AISM2008)*, pp. 152-157, 2008.
- [3] L. Shigang, “Monitoring Around a Vehicle by a Spherical Image Sensor,” *IEEE Trans. on Intelligent Transportation Systems*, 7, pp. 541-550, 2006.
- [4] L. Shigang and Y. Shimomura, “Lane marking detection by side Fisheye Camera,” *Proc. of IEEE/RSJ Int. Conf. on Intelligent Robots and Systems (IROS2008)*, pp. 606-611, 2008.
- [5] S. Gehrig, C. Rabe, and L. Krueger, “6D Vision Goes Fisheye for Intersection Assistance,” *Proc. of Canadian Conf. on Computer and Robot Vision (CRV2008)*, pp. 34-41, 2008.
- [6] Nissan Motor Co. Ltd., http://www.nissan-global.com/EN/NEWS/2007/_STORY/071012-01-e.html
- [7] T. Nishimoto and J. Yamaguchi, “Three dimensional measurement using fisheye stereo vision,” *Proc. of SICE Annual Conf. 2007*, pp. 2008-2012, 2007.
- [8] D. Xiaoming, W. Fuchao, W. Yihong, and W. Chongwei, “Automatic spherical panorama generation with two fisheye images,” *Proc. of 7th World Congress on Intelligent Control and Automation (WCICA2008)*, pp. 5955-5959, 2008.
- [9] R. Okutsu, K. Terabayashi, Y. Aragaki, N. Shimomura, and K. Umeda, “Generation of Overhead View Images by Estimating Intrinsic and Extrinsic Camera Parameters of Multiple Fish-Eye

Cameras,” Proc. of IAPR Conf. on Machine Vision Applications (MVA2009), 2009.

- [10] B. Triggs, P. McLauchlan, R. Hartley, and A. Fitzgibbon, “Bundle Adjustment -A Modern Synthesis.” Vision Algorithms: Theory & Practice, Springer-Verlag LNCS 1883, 2000.
- [11] J. Y. Bouguet, “Pyramidal Implementation of the Lucas Kanade Feature Tracker Description of the Algorithm,” OpenCV, Intel Corporation, 2000.
- [12] D. G. Lowe, “Object Recognition from Local Scale Invariant Features,” Proc. of IEEE Int. Conf. on Computer Vision (ICCV), pp. 1150-1157, 1999.
- [13] W. H. Press, S. A. Teukolsky, W. T. Vetterling, et al., “Numerical Recipes in C,” Cambridge University Press, Cambridge, pp. 408-412, 1992.
- [14] R. I. Hartley, “In Defense of the Eight-Point Algorithm,” IEEE Trans. on Pattern Analysis and Machine intelligence, Vol.19, No.6, pp. 580-593, 1997.
- [15] M. A. Fischler and R. C. Bolles, “Random Sample Consensus: A Paradigm for Model Fitting with Applications to Image Analysis and Automated Cartography,” Communications of the ACM, Vol.24, No.6, pp. 381-395, 1981.
- [16] J. Kannala and S. S. Brandt, “A generic camera model and calibration method for conventional, wide-angle, and fish-eye lenses,” Vol.28, No.8, pp. 1335-1340, 2006.



Name:
Hisanori Mitsumoto

Affiliation:
Toyota Motor Corporation

Address:
375-1 Imazato, Susono, Shizuoka 410-1104, Japan

Brief Biographical History:
2009 Received M. Eng. in precision engineering from Chuo University
2009- Joined Toyota Motor Corporation

Membership in Academic Societies:
• The Robotics Society of Japan (RSJ)



Name:
Toru Morita

Affiliation:
Course of Precision Engineering, Graduate School of Science and Engineering, Chuo University

Address:
1-13-27 Kasuga, Bunkyo-ku, Tokyo 112-8551, Japan

Brief Biographical History:
2008 Received B. Eng. in precision mechanics from Chuo University



Name:
Kenji Terabayashi

Affiliation:
Assistant Professor, Department of Precision Mechanics, Chuo University

Address:
1-13-27 Kasuga, Bunkyo-ku, Tokyo 112-8551, Japan

Brief Biographical History:
2004 Received M. Eng. degree in systems and information engineering from Hokkaido University
2008 Received Ph.D. degree in precision engineering from the University of Tokyo
2008- Assistant Professor at Chuo University

Main Works:
• K. Terabayashi, N. Miyata, and J. Ota, “Grasp Strategy when Experiencing Hands of Various Sizes,” eMinds: Int. J. on Human-Computer Interaction, Vol.1, No.4, pp. 55-74, 2008.

Membership in Academic Societies:
• The Robotics Society of Japan (RSJ)
• The Japan Society for Precision Engineering (JSPE)
• The Japan Society of Mechanical Engineers (JSME)
• The Virtual Reality Society of Japan (VRSJ)
• The Institute of Image Electronics Engineers of Japan (IIEEJ)
• The Institute of Electrical and Electronics Engineers (IEEE)



Name:
Yohei Aragaki

Affiliation:
Nissan Motor Co., Ltd.

Address:
1-1 Morinosatoayama, Atsugi-shi, Kanagawa 243-0123, Japan

Brief Biographical History:
1999- Joined Nissan Motor Co., Ltd.



Name:
Noriko Shimomura

Affiliation:
Nissan Motor Co., Ltd.

Address:

1-1 Morinosatoayama, Atsugi-shi, Kanagawa 243-0123, Japan

Brief Biographical History:

1991- Joined Nissan Motor Co., Ltd.

2003 Received Ph.D. degree in Engineering from Yokohama National University

Membership in Academic Societies:

- The Institute of Electronics, Information and Communication Engineers (IEICE)
 - The Institute of Electrical Engineers of Japan (IEEJ)
-



Name:
Kazunori Umeda

Affiliation:
Professor, Department of Precision Mechanics,
Chuo University

Address:

1-13-27 Kasuga, Bunkyo-ku, Tokyo 112-8551, Japan

Brief Biographical History:

1994 Received Ph.D. degree in precision machinery engineering from the University of Tokyo

1994- Lecturer at Chuo University

2003-2004 Visiting Worker at National Research Council of Canada

2006- Professor at Chuo University

Main Works:

- N. Hikosaka, K. Watanabe, and K. Umeda, "Development of Obstacle Recognition System of Humanoids Using Relative Disparity Maps from Small Range Image Sensors," J. Robotics and Mechatronics, Vol.19, No.3, pp. 290-297, 2007.
- M. Tateishi, H. Ishiyama, and K. Umeda, "A 200Hz Small Range Image Sensor Using a Multi-Spot Laser Projector," Proc. of IEEE Int. Conf. on Robotics and Automation, pp. 3022-3027, 2008.

Membership in Academic Societies:

- The Robotics Society of Japan (RSJ)
 - The Japan Society for Precision Engineering (JSPE)
 - The Japan Society of Mechanical Engineers (JSME)
 - The Horological Institute of Japan (HIJ)
 - The Institute of Electronics, Information and Communication Engineers (IEICE)
 - Information Processing Society of Japan (IPSJ)
 - The Institute of Electrical and Electronics Engineers (IEEE)
-